Antiferromagnetic cubic anisotropy governed exchange bias in CoFeB/IrMn bilayers

Chenyu Zhang,[1,2] Xinwei Feng,[3] Qingfeng Zhan,[3,*] and Yong Hu ●[1,2,†]

[1]*Department of Physics, College of Sciences, Northeastern University, Shenyang 110819, China*
[2]*State Key Laboratory of Rolling and Automation, Northeastern University, Shenyang 110819, China*
[3]*Key Laboratory of Polar Materials and Devices (MOE) and State Key Laboratory of Precision Spectroscopy,*
School of Physics and Electronic Science, East China Normal University, Shanghai 200241, China

Dependence of exchange bias (EB) on field-measuring direction is commonly studied to establish the relationship between unidirectional and magnetocrystalline anisotropies in ferromagnet/antiferromagnet (AFM) systems, and phenomenologically, a cosine series expansion with/without higher-order odd terms may be used to fit the experimental data. The role higher-order AFM anisotropy plays on EB and the reason for the existence of higher-order odd terms in the expansion are still ambiguous. Herein, the influence of AFM cubic anisotropy on EB and coercivity was studied in amorphous-CoFeB/epitaxially grown IrMn bilayers, based on experimental measurements and Monte Carlo simulations. The results show that EB is still unidirectionally symmetric with respect to the field-measuring direction, and the symmetric axis is parallel to the field-cooling (FC) direction. Monte Carlo simulation results evidence large enough AFM anisotropy capable of trapping the AFM spins in one of the easy-axis directions closest to the FC direction. These findings, on the one hand, reveal an EB mode with orthogonal major and minor axes by modifying the energy wells and thus patterning the spin alignments of the AFM IrMn layer by means of AFM in-plane fourfold anisotropy in layered thin films, external cooling, and measuring magnetic fields and, on the other hand, are an important step toward a complete microscopic understanding of EB.

I. INTRODUCTION

Exchange bias (EB), also known as unidirectional exchange anisotropy, commonly occurs at the interface between a ferromagnet (FM) and an antiferromagnet (AFM) by cooling the FM/AFM system under an applied field (H_{FC}) through the Néel temperature of the AFM (the temperature at which the AFM order sets in). Since its discovery, EB has been of great technological importance in tailoring the operating characteristics of most magnetic devices such as magnetic recording read heads, magnetic random access memories, and EB magnetic tunnel junctions (MTJs) due to the advantage of effectively pinning the FM magnetization in magnetic multilayers [1,2]. Moreover, from fundamental interest, EB can be used to determine the AFM surface order parameter [3], which is a probe of the interface magnetic exchange interactions that are otherwise difficult to measure. Measurements of the FM magnetization reversal in EB systems as a function of the in-plane angle of applied field with respect to the unidirectional anisotropy direction have been reported to get a better understanding of the relationship between EB and anisotropies [4–9]. An initial insight into the problem came from Meiklejohn and Bean (the M-B model) [1,4], who proposed an anisotropy energy term of $K_E \cos \varphi$ to account for the shifted hysteresis loop, where $K_E = H_E / M_{FM}$, and φ

is the angle between the FM magnetization (M_{FM}) direction and the EB field (H_E) direction dictated by field cooling (FC). This should lead to a simple $\cos \varphi$ dependence for $H_E(\varphi)$, which has also been found in amorphous-CoMoB/CoO [5] and amorphous-FeNiB/CoO bilayers [6], respectively.

On the contrary, a more general cosine series expansion with higher-order odd terms seems necessary to explain the experimentally observed data in some crystal systems such as FeNi/CoO [7,8] and FeNi/CrMnPt bilayers [9]. Theoretically, Geshev *et al.* [10] calculated the angular dependence of H_E derived from the hysteresis loop measurements in FM/AFM bilayers in the framework of a phenomenological model that considers both rotatable and nonrotatable contributions to AFM layer anisotropy. The inclusion of rotatable anisotropy changes the shape and characteristics of the magnetization curve. The larger the relative contribution of the rotatable anisotropy to the effective uniaxial anisotropy, the closer the loop shift angular variation gets to a pure cosine behavior, opposite to the conclusion drawn by Krivorotov *et al.* [11] in Fe/MnF$_2$ bilayers experimentally that the high-order terms in the Fourier expansion of EB vs angle originate from the nonrigid AFM spin structure. Furthermore, Jiménez *et al.* [12] compared the angular dependencies of EB from two FM layers with different intrinsic anisotropies and found that the suppression of FM anisotropy also favors obtaining a simple $\cos \varphi$ dependence of H_E. Remarkably, much research focused on the correlation between EB and FM anisotropies involving high-order terms [13], and the role AFM cubic anisotropy plays on EB has not been reported yet.

*qfzhan@phy.ecnu.edu.cn
†huyong@mail.neu.edu.cn

On the other hand, to establish a link between the tailored vectorial magnetization switching process and EB with high-order AFM anisotropies via FM/AFM interfacial coupling, it is highly desirable to investigate the feasibility of incorporating amorphous FM alloys where the magnetocrystalline ordering is absent to exhibit very soft magnetic properties, higher electrical resistivity, and better corrosion resistance, and a very wide composition range can be tailored in exchange-coupled FM/AFM structures [5]. For the AFM, clean anisotropies with low dispersions are favored to appear in epitaxial films or single crystals, and fully epitaxial stacks allow for the maximum control of properties. Zhang and Krishnan [14] summarized the recent progress of epitaxial EB systems and presented an outlook on how, in this paper on epitaxial EB systems, we could shed light on the future developments in AFM spintronics. Using more advanced compounds has been suggested, as these can exhibit a range of exciting properties related to EB [14–24]. For example, epitaxial growth of Fe_3O_4/CoO superlattices and NiO/Fe(001) films has been demonstrated, and it has revealed that the AFM spins are preferentially frozen perpendicular to the FM spins at low temperature below a critical temperature [15,16]. In single-crystal FeF_2, zero EB was observed along the FC direction for a well uncompensated interface of $FeF_2(001)$ or $FeF_2(100)$, while perpendicular coupling observed for a compensated $FeF_2(110)$ interface also produced rather small EB, implying hindered spin canting due to large AFM anisotropy [17]. Moreover, the conventional square and the unusual two-step EB hysteresis loops were obtained in a-axis oriented PdMn/Fe bilayers [18], while in c-axis oriented PdMn/Fe bilayers, asymmetrical multistep loops may also be observed [19]. The study of polarized neutron reflectivity has interpreted that the differences of the surface compensation in different orientations give rise to different FM/AFM coupling and magnetic reversal properties once the AFM is exchange-coupled to a FM layer [20]. In epitaxial IrMn/Fe bilayers [14,21,22], several kinds of multistep loops were observed for the samples measured at various field orientations, and EB at room temperature was induced by applying a small magnetic field without postannealing. Furthermore, transitions of H_E from a negative field to a positive field with increasing time scale have been reported in epitaxial IrMn/CoFe bilayers [23]. Our previous work [24,25] has also reported in-plane fourfold symmetric coercivity (H_C) in an amorphous CoFeB layer, which was imprinted by an epitaxial FeRh layer with cubic anisotropies.

Finally, H_{FC} is also crucial for the determination of the magnetization switching process and EB direction [26]. This called for a systematic study on the magnetization reversal asymmetry as to different directions of the in-plane H_{FC} and measuring field with respect to the AFM easy-axis direction. Many material systems have been developed for both the fundamental understanding of physics and technological applications. CoFeB/IrMn is an ideal system for EB MTJs due to the high thermal stability and high blocking temperature of IrMn. The CoFeB alloys show excellent soft magnetic behaviors, and the resultant high spin polarization makes CoFeB extensively applied in multilayered spintronic devices [27–29]. As of today, CoFeB/IrMn has emerged as one of the most important material systems in spintronic de-

vices [30–35]. In this paper, we study the role fourfold AFM magnetocrystalline anisotropy plays on EB and coercivity in amorphous-CoFeB/epitaxially grown IrMn bilayers, where uniaxial magnetic anisotropy in the amorphous CoFeB layer is rather weak, and the IrMn layer is epitaxially grown on the MgO(001) substrate, based on the measurements of longitudinal and transverse magneto-optic Kerr effect (MOKE) magnetometry and Monte Carlo calculations.

II. METHODS

A. Experimental details

IrMn/CoFeB bilayers with IrMn thickness of 30 nm and CoFeB thickness of 10 nm were deposited on the commercial (001)-oriented MgO substrate [see Fig. 1(a)] by a magnetron sputtering system with a base pressure $<1.0 \times 10^{-8}$ Torr. The substrate was annealed at 500 °C for 1 h in a vacuum chamber. Then the IrMn layer was epitaxially grown at 500 °C and annealed at 500 °C for 1 h. After cooling down to room temperature, the CoFeB layer was deposited on top of the IrMn layer. A magnetic field of 500 Oe provided by a permanent magnet was applied along the MgO[110] axis during growth to induce EB parallel to IrMn[110], based on the epitaxial relationship of IrMn(001)[110]||MgO(001)[110]. Before being taken out of the vacuum chamber, a 3 nm Ta capping layer was used to prevent the films from oxidation. To realign the EB along the IrMn[100] direction, the sample was heated up to 300 °C, held for half an hour, and then naturally cooled to room temperature in the vacuum chamber with a magnetic field of 500 Oe applied along the MgO[100] direction. The film thicknesses were controlled by deposition time, which have been calibrated by x-ray reflectivity (XRR). The crystal structure was analyzed by x-ray diffraction (XRD). The magnetic hysteresis loops were measured at room temperature by using a self-built MOKE setup. The longitudinal Kerr signal was recorded by illuminating the sample from the top side with a He-Ne laser light ($\lambda = 633$ nm). The orientation of the magnetic field was changed at an interval of 10° by rotating the sample in the plane of the film. The FM resonance (FMR) absorption spectra of the bilayer were obtained at room temperature by using a Bruker EMX-plus 10/12 spectrometer at a radiofrequency of 9.31 GHz. An in-plane magnetic field swept from 0 to 2000 Oe was applied with respect to the IrMn[100] direction at an interval of 10°.

B. Monte Carlo simulation

To interpret the experimental results of the angular (φ) dependencies of H_E and H_C in CoFeB/IrMn bilayers, meanwhile, to present a correspondence between magnetization reversal processes, $H_E(\varphi)$ behaviors, and microscopic AFM spin configurations at the FM/AFM interface, Monte Carlo simulations with a modified Metropolis algorithm are performed. Regardless of the actual spin structures of CoFeB and IrMn layers at the interface, which remain unknown, a coarse-grained model is used, where $100 \times 100 \times [2(t_{CoFeB}) + 2(t_{IrMn})] = 40\,000$ spins are placed on the node of simple cubic lattice, with periodic boundary conditions considered in the lateral (xy plane) directions and open in the z direction. In the presence of a magnetic field, the Hamiltonian of the
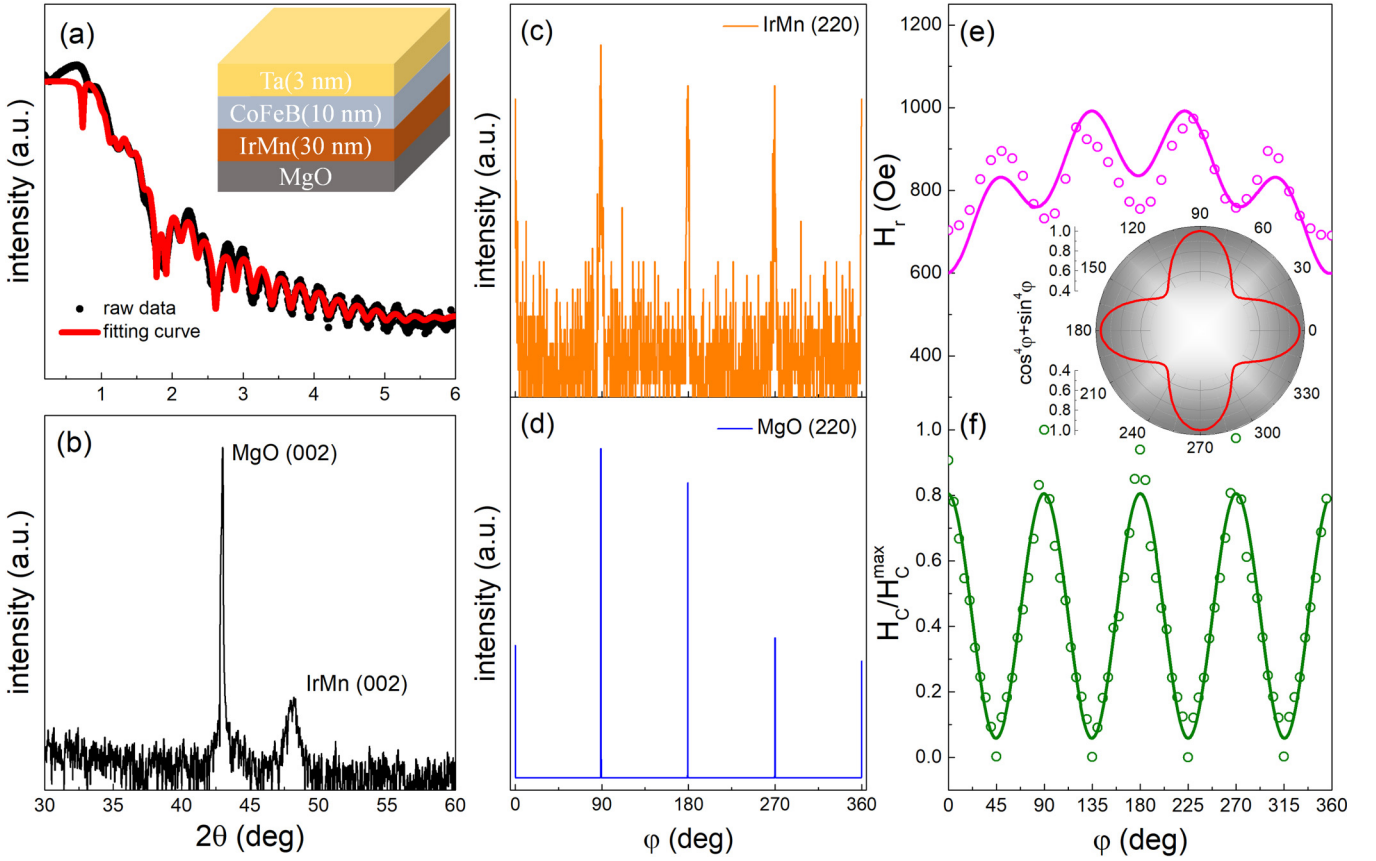
FIG. 1. (a) X-ray reflectivity experimental data (black dots) for the CoFeB/IrMn bilayer and the corresponding fitting curve (red line). The inset schematically shows the layered structure of the sample. (b) X-ray θ-2θ scan for the CoFeB/IrMn bilayer. X-ray in-plane φ scans for (c) the epitaxial IrMn layer and (d) the MgO(001) substrate. (e) Angular dependence of resonance field H_r obtained by the ferromagnetic resonance (FMR) measurements. (f) The calculated coercivity, normalized by the maximum value, as a function of φ. The inset shows the in-plane fourfold anisotropy of the epitaxial IrMn layer.

bilayer is written as

$$\mathcal{H} = - \sum_{<ij\in\mathrm{CoFeB>}} J_{\mathrm{CoFeB}}(S_i \cdot S_j)$$
$$- \sum_{i\in\mathrm{CoFeB}} K_{\mathrm{CoFeB}}\left(S_i \cdot \hat{e}_K^{\mathrm{CoFeB}}\right)^2$$
$$- \sum_{<ij\in\mathrm{IrMn>}} J_{\mathrm{IrMn}}(S_i \cdot S_j) - \sum_{i\in\mathrm{IrMn}} K_{\mathrm{IrMn}}\left[\left(S_i^x\right)^4 + \left(S_i^y\right)^4\right]$$
$$- \sum_{<i\in\mathrm{CoFeB},j\in\mathrm{IrMn>}} J_{\mathrm{CoFeB/IrMn}}(S_i \cdot S_j)$$
$$- \sum_i HM_S(S_i \cdot \hat{e}_H), \tag{1}$$

where S_i denotes the unit vector of spin i. The first line in Eq. (1) gives the FM exchange and uniaxial anisotropy energy terms, where J_{CoFeB} and K_{CoFeB} are the FM exchange and anisotropy constants, the angular bracket denotes the summation over the nearest-neighbor pairs only, and $\hat{e}_K^{\mathrm{CoFeB}}$ is the unit vector of the FM easy-axis direction. The second line gives the AFM energy contributions with the AFM exchange (J_{IrMn}) and cubic anisotropy (K_{IrMn}) constants. Due to the nature of the interface, only the in-plane components of K_{IrMn} are considered, and the easy-axis directions are set along the

x ([100] and [-100]) and y ([010] and [0-10]) directions. The last line presents the FM/AFM interfacial exchange energy and the Zeeman energy, where $J_{\mathrm{CoFeB/IrMn}}$, H, M_S, and $\hat{e}_H$ are the interfacial exchange constant, the magnetic field, the saturation magnetization, and the unit vector of magnetic-field direction, respectively.

For the soft FM CoFeB, $J_{\mathrm{CoFeB}} = 10\,\mathrm{meV}$, $M_S = 1.2 \times 10^6\,\mathrm{A\,m^{-1}}$ [28,29], and $\hat{e}_K^{\mathrm{FM}} = \hat{e}_H$ are set when the magnetizing direction changes. For the hard AFM IrMn, a locally nonzero uncompensated magnetization component at the CoFeB/IrMn interface and high K_{IrMn} are both crucial for EB, and thus, J_{IrMn} is set by a small value, i.e., $J_{\mathrm{IrMn}} = -1\,\mathrm{meV}$, to encourage the appearance of large-area parallel spin domains in the AFM layer at the target temperature after FC. On the other hand, K_{CoFeB} and K_{IrMn} are both adjustable parameters to fit and study the experimental EB results. Furthermore, $J_{\mathrm{CoFeB/IrMn}} = 5\,\mathrm{meV}$ is used and much larger than the real values when the simulation EB results fit well with the experimental one since a size-scaling technique based on the micromagnetism approximation has been applied [36,37].

The simulation procedure mimics the experimental one. The initial state of the bilayer model is magnetically disordered, and then the model is cooled from a high enough temperature of 600 K, where the AFM layer is superparamagnetic, down to 300 K under a cooling field of 2 T, which is

applied along the [100] or [110] directions to determine the unidirectional anisotropy (K_{eb}) direction. At 300 K, the hysteresis loop is recorded by cycling the magnetic field between -300 and 300 Oe. Then the magnetic field counterclockwise rotates by 5°, and the hysteresis loop is rerecorded. We define φ as the angle between the magnetic field and [100] directions, and φ is varied between 0° and 355° in increments of 5°. The Monte Carlo Metropolis algorithm is used to determine the evolution of spin, and at each Monte Carlo step, the spin energies are exactly calculated based on the Stoner-Wohlfarth model to judge whether the spin flip occurs to avoid an unphysical tunneling [38,39]. At each temperature or magnetic field, 1.0×10^5 Monte Carlo steps are used to equilibrate the system, followed by another 1.0×10^5 Monte Carlo steps to average the quantities such as magnetization, magnetic energy, and spin configuration. Finally, 50 sets of independently and randomly initial states are used to calculate the final simulation results to minimize the calculation errors, and thus, the error bars are not plotted in the figures.

III. RESULTS

Figure 1(a) shows the XRR data for the CoFeB/IrMn bilayer sample. The corresponding fitting result indicates the thicknesses of IrMn, CoFeB, and Ta are 32.1, 10.1, and 3.3 nm, respectively. The IrMn(002) and MgO(002) peaks are observed in the XRD pattern, indicating the (001) growth orientation of IrMn on the MgO(001) substrate, as shown in Fig. 1(b). No CoFeB peak is detected due to the amorphous structure. The x-ray in-plane φ scans reveal the cube-on-cube epitaxial growth of IrMn on MgO with a relationship of IrMn(001)[110]||MgO(001)[110], as shown in Figs. 1(c) and 1(d). Figure 1(e) presents the angular dependence of the resonance field H_r obtained by the FMR measurements for the CoFeB/IrMn bilayer with the EB aligned along the MgO[100] direction. They can be well fitted by using a simplified equation derived from the Landau-Lifshitz equation by considering a fourfold magnetic anisotropy K_1, a uniaxial magnetic anisotropy K_u, and a unidirectional anisotropy K_{eb} [15,40]:

$$
\left(\frac{\omega}{\gamma}\right)^2 = \left[H_r + 4\pi M_S - \frac{3K_1}{2M_S} + \frac{2K_u}{M_S}\cos(2\varphi) \right.
$$
$$
\left. + \frac{K_1}{2M_S}\cos(4\varphi) + \frac{K_{eb}}{M_S}\cos(\varphi) \right]
$$
$$
\times \left[H_r + \frac{4K_u}{M_S}\cos(2\varphi) \right.
$$
$$
\left. + \frac{2K_1}{M_S}\cos(4\varphi) + \frac{K_{eb}}{M_S}\cos(\varphi) \right], \qquad (2)
$$

where $\frac{\omega}{2\pi}$ is the microwave excitation frequency, and γ is the gyromagnetic ratio. Consequently, the anisotropic field parameters of $\frac{K_1}{M_S} = 44\,\text{Oe}$, $\frac{K_u}{M_S} = 6\,\text{Oe}$, and $\frac{K_{eb}}{M_S} = 118\,\text{Oe}$ are obtained, which indicate that EB gives rise to not only the well-known unidirectional and uniaxial anisotropies but also in-plane fourfold magnetic anisotropy in the amorphous CoFeB layer because of the epitaxially grown IrMn layer. In the Monte Carlo simulations, the angular dependence of H_C in the CoFeB/IrMn bilayers after zero FC (without EB)

is firstly studied with the results presented in Fig. 1(f). The results show that the maximum H_C is obtained along the easy-axis directions (0°, 90°, 180°, and 270°), while the minimum H_C obtained in the hard-axis directions (45°, 135°, 225°, and 315°), analogous to the coercivity behaviors reported in the CoFeB/FeRh bilayers previously [24,25], where in-plane fourfold anisotropy in the AFM layer can be imprinted on the angular dependence of H_C in the amorphous CoFeB layer. Unfortunately, the EB effect is not observed in the CoFeB/FeRh bilayers even if a cooling field is added, and this paper provides an opportunity to study the role AFM in-plane fourfold anisotropy plays on EB in the CoFeB/IrMn bilayers.

Figures 2(a) and 2(c) depict the representative hysteresis loops experimentally measured at different φ at room temperature for the bilayers with K_{eb} parallel to the [100] and [110] directions, respectively. When K_{eb} is parallel to the [100] direction, i.e., the magnetizing direction at $\varphi = 0°$ is along with K_{eb} and one of the easy axes of K_1, the loop is square-shaped and shifts to the negative field direction. As φ increases to 45°, the magnetization reversal becomes rounded, and the loop exhibits an S shape and moves to the right while still shifting to the negative field direction. At $\varphi = 90°$, where the magnetizing direction is along another easy axis of K_1 and orthogonal to K_{eb}, the loop becomes symmetric about the field axis, the magnetization nearly linearly decreases with decreasing magnetic field under weak fields. When K_{eb} is parallel to the [110] direction, it is noteworthy that $\varphi = 0°$ is also defined when the magnetizing direction is along the [100] direction, the same as $K_{eb}||[100]$ for comparison. Thus, the widest, square-shaped loop with a shift to the negative field direction is observed at $\varphi = 45°$. The loops obtained at $\varphi = 90°$ and 135° are like that at $\varphi = 45°$ and 90° for $K_{eb}||[100]$.

As shown in Figs. 2(a) and 2(c), the FM easy-axis direction, identified by obtaining the square-shaped loop, is always roughly parallel to the FC direction, even though the FC direction overlaps one of the AFM easy-axis directions. Thus, the so-called spin-flop coupling, commonly induced in epitaxial EB systems to result in a two-step reversal characteristic [15,17,41–43], seems not to exist in the present CoFeB/IrMn bilayers. Spin-flop coupling refers to the perpendicular arrangement of FM and AFM spins at the interface and intuitively arises from the long-range ordering of a compensated interface since an orthogonal FM/AFM arrangement is a natural consequence, as it minimizes the frustration of exchange coupling from the two AFM sublattices [14]. Nevertheless, exceptions were also proposed; for example, in epitaxial Fe/MnPd bilayers, Zhang and Krishnan [44] found a transition from the perpendicular FM/AFM coupling to the collinear FM/AFM coupling for the MnPd thickness <30 nm or the temperature >90 K, and this spin-reorientation transition was physically attributed to competing effects between the interface-induced-uniaxial anisotropy and intrinsic FM anisotropy [45]. Moreover, a globally compensated matrix with local uncompensated clusters exhibiting net moments due to a strong interfacial exchange coupling [46] or a strong AFM/external-magnetic-field coupling [47] may also favor forming collinear FM/AFM anisotropies. Therefore, the types of FM/AFM coupling in epitaxial EB systems can be determined by the interplay between the intrinsic
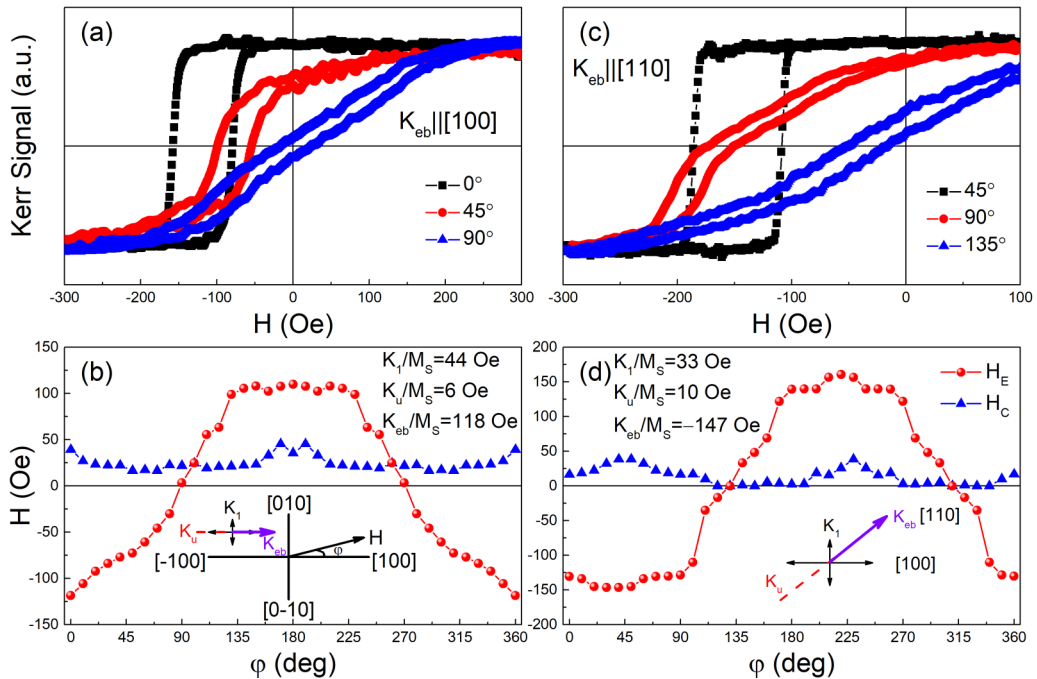
FIG. 2. Typical longitudinal magneto-optic Kerr effect (MOKE) loops measured at various field orientations when K_{eb} is set along the (a) [100] and (c) [110] directions. (b) and (d) Exchange bias field (H_E) and coercivity (H_C) as a function of φ. The insets show the magnetic field orientation and different easy-axis directions with respect to the in-plane x and y axes.

FM/AFM anisotropies and the external magnetic field. In amorphous-CoFeB/epitaxially grown IrMn bilayers, the magnetocrystalline anisotropy of the amorphous CoFeB layer is considered negligible [24]. Furthermore, the interfacial exchange coupling between CoFeB and IrMn layers and the cooling field both play dominant roles in inducing uncompensated spins that exist on the surface of the epitaxial IrMn layer. Thirdly, the given IrMn thickness and temperature may also be responsible for no spin-flop coupling observed in CoFeB/IrMn bilayers.

The loop variation with φ is further quantified through calculating $H_E = (H_R + H_L)/2$ and $H_C = (H_R - H_L)/2$, where H_R and H_L are the coercive fields at the ascending and descending branches of a loop. For $K_{eb}||[100]$ shown in Fig. 2(b), H_E gets maximum values in the negative field direction around $\varphi = 0°$ and then rapidly decreases in the negative field direction and increases in the positive field direction when φ increases to 135° and $H_E(90°) \sim 0$. At $\varphi = 135°–225°$, H_E nearly levels off at the highest positive value and then H_E drops down as φ further increases from 225° and changes its sign around $\varphi = 270°$. On the contrary, the H_C behaviors are insensitive to φ, while H_C kicks up around $\varphi = 0°$ and 180°. Remarkably, the φ dependence of H_E exhibits a unidirectional symmetry, while that of H_C is uniaxially symmetric. However, this dependence of H_E on φ deviates from a pure $\cos\varphi$ relation [4–6] due to the nonnegligible roles of K_1 played in the hard-axis directions (45°, 135°, 225°, and 315°), which is confirmed by the FMR measurements. To distinguish the roles played by K_{eb} and K_u on the H_E vs φ behaviors, H_E and H_C as a function of φ for $K_{eb}||[110]$ are also studied and shown in Fig. 2(d). The maximum values of H_E in the negative and positive field directions occur at $\varphi = 0°-90°$ and $180°-270°$, respectively, and zero H_E appears around $\varphi = 135°$ and $315°$. Meanwhile, H_C kicks up around $\varphi = 45°$ and 225°. Remarkably, the φ dependence of H_E and H_C for $K_{eb}||[110]$ both shift by 45° with respect to $K_{eb}||[100]$, designating that the symmetric axes of H_E and H_C in the CoFeB/IrMn bilayers mainly depend on the cooling field direction, i.e., K_{eb}. Furthermore, the φ dependence of H_E is still unidirectionally symmetric, concomitant with a uniaxially symmetric H_C behavior against φ. Thus, the in-plane fourfold anisotropy of IrMn induces higher-order terms, while the uniaxial anisotropy of CoFeB plays a minor role.

Next, the calculated hysteresis loops recorded along different magnetizing directions and the H_E and H_C behaviors with increasing φ at room temperature based on the Monte Carlo simulations are presented in Fig. 3. For $K_{eb}||[100]$, seen in Fig. 3(a), the widest square-shaped loop appears at $\varphi = 0°$ and with increasing φ, the descending branch moves to the right, while the ascending branch initially moves to the left from $\varphi = 0°$ to 45° and then turns to the right from $\varphi = 45°$ to 90°. Moreover, the obvious shift of the loop is observed at $\varphi = 0°$ and 45°, while the most rounded loop with no shift appears at $\varphi = 90°$. As shown in Fig. 3(b), H_E is maximum in the negative field direction around $\varphi = 0°$, and decreases down to zero with increasing φ from 0° to 90°. With increasing φ from 90° to 180°, H_E increases in the positive field direction from zero to the maximum value. When φ further increases from 180° to 360°, H_E decreases in the positive field direction to zero at $\varphi = 270°$ and increases to a maximum value in the negative field direction. Meanwhile, the maximum values of H_E exhibit a small plateau around $\varphi = 0°$ and 180°. On the other hand, H_C exhibits peaks at $\varphi = 0°$ and 180°, while H_C fluctuates around the minimum value between $\varphi = 45°$ and 135° and between 225° and 315°. For $K_{eb}||[110]$, the widest square-shaped loop appears at $\varphi = 45°$, while the most
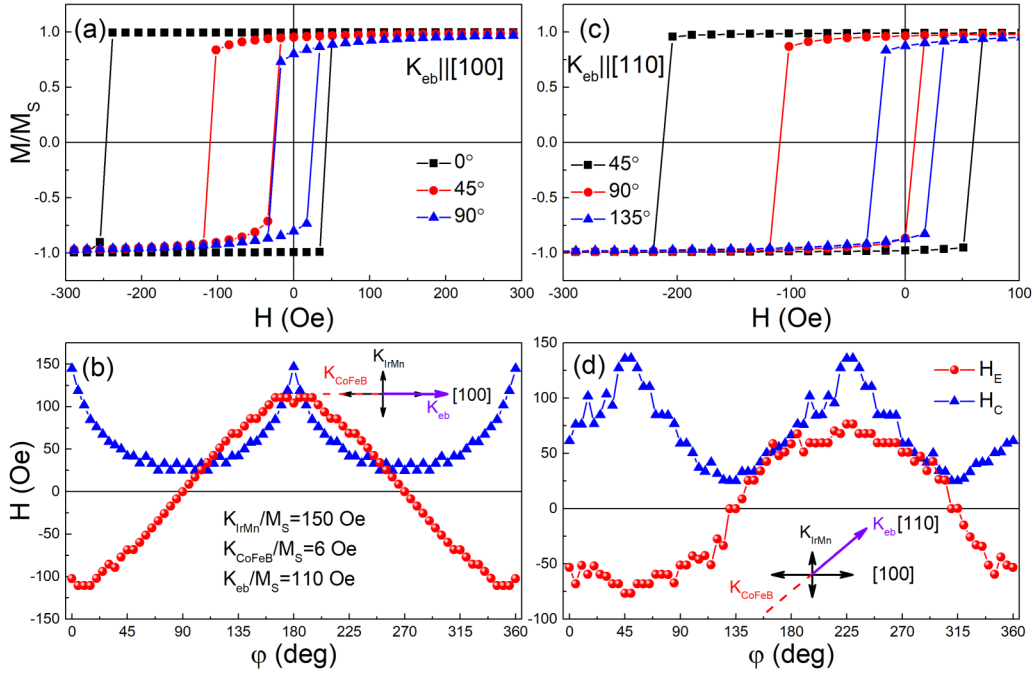
FIG. 3. Calculated hysteresis loops measured at various field orientations when K_{eb} is set along the (a) [100] and (c) [110] directions. (b) and (d) Exchange bias field (H_E) and coercivity (H_C) as a function of φ. The insets show the magnetic field orientation and different easy-axis directions with respect to the in-plane x and y axes. The fitting values of IrMn cubically (K_{IrMn}/M_S), CoFeB uniaxially anisotropic fields (K_{CoFeB}/M_S), and the measurement value of the unidirectionally anisotropic fields (K_{eb}/M_S) are presented.

rounded loop with no shift is obtained at $\varphi = 135°$. In other words, the H_E and H_C behaviors with φ for $K_{eb}||[110]$ shift by 45° as compared with $K_{eb}||[100]$.

The calculated φ dependence of H_E and H_C are qualitatively consistent with the experimental results, reminiscent of the validity of the model and simulation method adopted to study the experimental findings. Furthermore, when $K_{eb}||[100]$ and $K_{eb}/M_S = 110$ Oe in the simulations approaches the experimental findings ($K_{eb}/M_S = 118$ Oe), $K_{CoFeB}/M_S = 6$ Oe is very consistent with the experimental fitting value of $K_u/M_S = 6$ Oe, while $K_{IrMn}/M_S = 150$ Oe is 3.4 times larger than that ($K_1/M_S = 44$ Oe) experimentally, indicating that the FM anisotropy is weakly influenced by the AFM layer, while only partial fourfold anisotropy of the AFM layer imprinted on the FM layer via their interface. The calculated H_C maximum value (~150 Oe) is also threefold higher than that (~50 Oe) observed in the experiment. The complex angular dependence of H_E and H_C and the discrepancy between experiments and theories were also reported in other epitaxial EB systems [48–51]. In epitaxial CoFe/IrMn bilayers, the hysteresis loop drastically changed from a normal magnetization process to an asymmetric double-shifted one due to the competition between comparable cubic crystalline and uniaxial anisotropies ~45° [48]. In addition, the deviations between experimental findings and theoretical fitting results were observed in the narrow angular ranges ~0° and 180° in epitaxial NiFe/FeMn(001) and Co/NiO(001) bilayers, which were interpreted by the possibility of domain formation and thermal activation to overcome the involved energy barriers [49,50]. Thirdly, Hajiri *et al.* [51] presented that the interface frustration and roughness in fully epitaxial Co_3FeN/MnN bilayers experimentally were responsible for

the discrepancy of the order of magnitude of H_E between calculation and experiment. Thus, the inconsistence of quantities between experimental and simulation results in this paper may also arise from the perfect CoFeB/IrMn interface model with a much smaller size that is considered in the simulation. However, the interface is never perfect even for the epitaxially grown bilayers. Roughness, deviations from stoichiometry, interdiffusion, structural defects, low spin coordination at surface sites, etc., cause nonideal magnetic interfaces, and it is therefore natural to assume that, on average, a fraction of AFM spins have lower anisotropy than the bulk ones [52,53].

IV. DISCUSSION

In EB systems, it is well known that different reversal pathways, corresponding to the coherent rotation and the domain wall nucleation, on each branch of the hysteresis loop, i.e., asymmetry, may be obtained and result in irreversible Barkhausen jumps [54,55]. Moreover, the FC and field-measuring treatments executed along different directions are effective to create two or more misaligned and competing anisotropies [56]. Therefore, a number of pairs of longitudinal ($M_{||}$) and transverse ($M_\perp$) components of magnetization were measured for an external field orientation with respect to the [100] direction ranging from 0° to 360°, with the representative results of $\varphi = 0°$, 45°, 90°, and 135° for $K_{eb}||[100]$ shown in Fig. 4. At $\varphi = 0°$, the $M_{||}$ loop with a square shape exhibits a shift toward the negative field direction, while the $M_\perp$ value always equals zero, indicating no existence of measurable nonzero components of magnetization during magnetization reversal. An asymmetric magnetization reversal at the descending and ascending branches is observed at $\varphi = 45°$ due
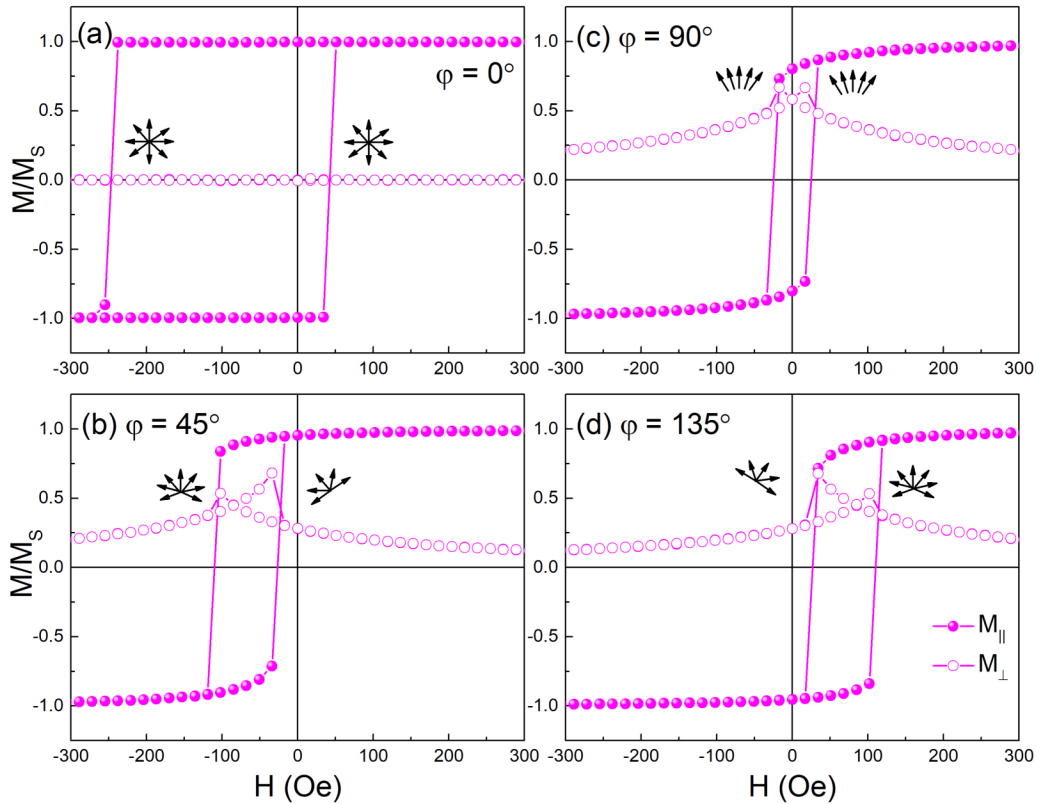
FIG. 4. Calculated longitudinal ($M_{\parallel}$) and transverse ($M_{\perp}$) components of hysteresis loops at selected φ for $K_{\text{eb}}||[100]$, where arrows indicate the schematic illustrations of spin configurations on the IrMn surface.

to different peak magnitudes of $M_{\perp}$, and the forward component of $M_{\perp}$ is lower than the reverse component. With the increase of φ to 90°, the $M_{\parallel}$ loop becomes completely symmetric, and this is also seen in the $M_{\perp}$ loop, where the forward and reverse components have the same nonzero magnitude. Finally, the $M_{\parallel}$ loop shifts to the positive field direction for $\varphi = 135°$, concomitant with an asymmetric reversal of the $M_{\perp}$ loop where the reverse component is lower.

At first, a collinearly coupled bilayer is identified because $M_{\perp}$ only reverses in one semicircle [57], and thus, the varied value of $M_{\perp}$ in the FM layer during the magnetization reversal of $M_{\parallel}$ can mirror the rotating AFM spins at the FM/AFM interface strongly depending on φ, which may be used to interpret the angular dependence of EB meanwhile to study the role of AFM anisotropy. A direct indication of the rotating AFM spins has been revealed experimentally by soft x-ray magnetic dichroism [53,58,59]. Element-specific hysteresis loops showed that some spins belonging to the AFM layer rotate reversibly with the FM spins. Due to the shift of the hysteresis loop, it is obvious that the other part of the AFM layer is frozen. Therefore, the AFM layer can be considered, to a first approximation, as consisting of two types of AFM states: one part having a large anisotropy preserving the AFM state and the other interfacial part with a weaker anisotropy, allowing the spins to rotate together with the FM spins. Hence, the features of the instant AFM spin configurations during FM magnetization reversals at selected φ values are schematically shown in Fig. 4, which is like the experimental findings of polarized neutron scattering in Co/CoO and CoFe/IrMn

bilayers, where the FM spins at the FM/AFM interface are not collinear with the applied field direction during the reversal, and the interface is disordered, containing domains and domain walls even in saturation, analogous to a spin-glass system [60–62].

By comparing the H_E and H_C behaviors with φ obtained from experiment (seen in Fig. 2) and simulation (seen in Fig. 3), the calculated values of H_C in the easy-axis directions are roughly triple those in the experiment. Both experimentally and theoretically, it is found that $H_E(\varphi)$ still stays unidirectionally symmetric even in the presence of a strong cubic AFM anisotropy, although it has been discussed that a cosine series expansion of $H_E(\varphi)$ should have higher-order odd terms. Next, the roles of K_{CoFeB} and K_{IrMn} on angular-dependent H_C and H_E have been studied to interpret the discrepancy mentioned above. As shown in Fig. 5(a), with decreasing K_{CoFeB}/M_S, the H_C values at $\varphi = 0°$ and 180° decrease monotonically, and the decrement of H_C is proportional to that of K_{CoFeB}, indicating the maximum values of H_C in the directions parallel or opposite to K_{eb} strongly depend on K_{CoFeB}. At $\varphi = 90°$ and 270°, H_C firstly decreases down to zero with decreasing K_{CoFeB}/M_S, and the further decrease of K_{CoFeB}/M_S results in a widening of the φ range where H_C equals zero. For the experimental results of H_C shown in Fig. 2(b), H_C is always nonzero, and its value with φ varies from $\sim$20 Oe around $\varphi = 90°$ and 270° to $\sim$50 Oe around $\varphi = 0°$ and 180°. Hence, the fitting value of $K_{\text{CoFeB}}/M_S = 6$ Oe is suitable for $\varphi = 90°$ and 270°, while the value of K_{CoFeB}/M_S at $\varphi = 0°$ and 180° should decrease
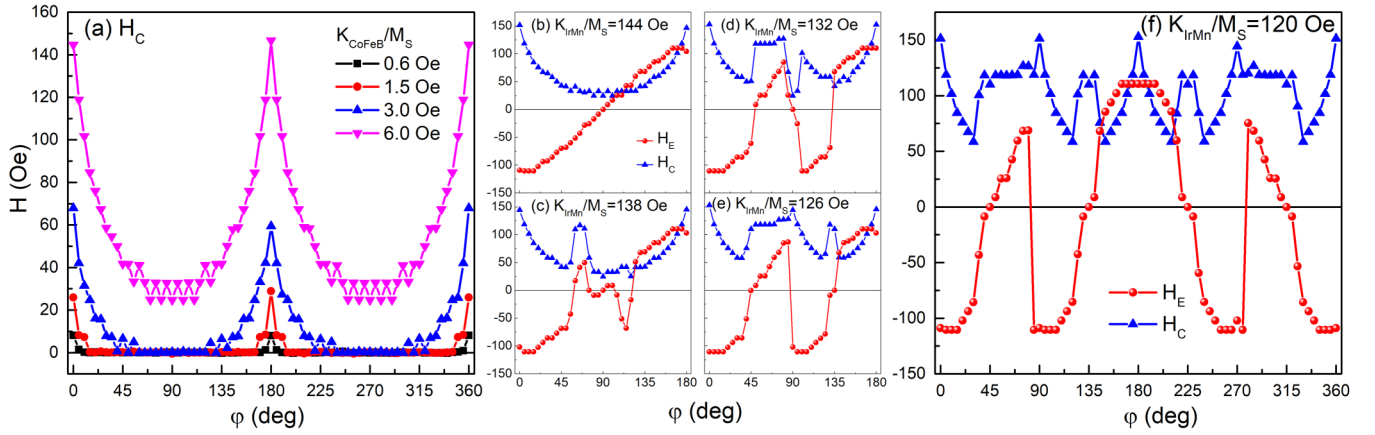
FIG. 5. (a) Coercivity (H_C) as a function of φ for selected values of ferromagnet (FM) anisotropic field (K_{CoFeB}/M_S). (b)–(f) Exchange bias field (H_E) and H_C as a function of φ for selected values of antiferromagnet (AFM) anisotropic field (K_{IrMn}/M_S). K_{eb} is pointing to the [100] direction.

to ~ 2 Oe to meet the experimental result of H_C. In other words, the nonzero H_C around $\varphi = 90°$ and $270°$ mainly originates from the contribution of FM anisotropy. The different values of K_{CoFeB}/M_S in the AFM orthogonal easy-axis directions probably arise from the distinct φ-related frozen AFM spin configurations at the FM/AFM interface after the FC process.

On the other hand, with decreasing K_{IrMn}/M_S, $H_E(\varphi)$ evolves from a monotonic function, where H_E varies from a negative minimum to a positive maximum with increasing φ from $0°$ to $180°$, to a nonmonotonic function, and at $K_{IrMn}/M_S = 120$ Oe, H_E increases from a negative minimum around $\varphi = 0°$, across zero at $\varphi = 45°$, and to a positive value with increasing φ. Then H_E drops down to the negative minimum value around $\varphi = 90°$ and increases again across zero at $\varphi = 135°$ and to a positive maximum around $\varphi = 180°$. The H_E behavior with increasing φ from $180°$ to $360°$ is mirror symmetric about the vertical axis of $\varphi = 180°$. Meanwhile, the behavior of H_C becomes complex with increasing φ and remains mirror symmetric about the vertical axis of $\varphi = 180°$. In other words, for a smaller K_{IrMn}/M_S value, the negative minimum and positive maximum of H_E still appear around $\varphi = 0°$ and $180°$, respectively, which are close to the easy-axis directions of K_{IrMn} parallel and antiparallel to K_{eb}, while near the easy-axis directions of K_{IrMn} orthogonal to K_{eb}, the H_E value exhibits a sharp drop/jump between negative values and positive values, and $H_E = 0$ is obtained in all hard-axis directions of K_{IrMn}, although the unidirectional symmetry of H_E behavior with φ remains. Meanwhile, H_C also exhibits weak fourfold symmetry with existence of peak values in all easy-axis directions. The deficit of AFM anisotropy energy favors its fourfold characteristics to be imprinted by the φ dependence of H_E and H_C, reminiscent of the energy competition between K_{IrMn} and $J_{CoFeB/IrMn}$ as well as the uncompensated AFM magnetization (M_{IrMn}) governed by K_{eb} which play crucial roles.

Figure 6 depicts the results of the φ dependence of normalized uncompensated AFM magnetization [$M_{IrMn}/M_{S(IrMn)}$], FM/AFM interfacial exchange energy density ($\varepsilon_{CoFeB/IrMn}$), and AFM anisotropy energy density (ε_K^{IrMn}) for selected

K_{eb} directions and K_{IrMn}/M_S values. For $K_{eb}||[100]$ and $K_{IrMn}/M_S = 150$ Oe, the calculated $M_{IrMn}/M_{S(IrMn)}$ value decreases monotonically from $+1$ to -1 with increasing φ from $0°$ to $180°$. Then the average AFM spin orientation at the FM/AFM interface is calculated by $\langle\varphi_{IrMn}\rangle = \sum_{i=1}^{N}\varphi_i/N$, and remarkably, $\langle\varphi_{IrMn}\rangle = \varphi$ is obtained with a reversible value of $M_{IrMn}/M_{S(IrMn)}$ under H_L and H_R for a given φ. Moreover, $\varepsilon_{CoFeB/IrMn}$ under H_L remains minimum when φ is $<45°$ and increases to the maximum with increasing φ to $180°$. On the contrary, $\varepsilon_{CoFeB/IrMn}$ under H_R decreases from the maximum to the minimum with increasing φ from $0°$ to $135°$ and then levels off for larger φ. The degenerate state under H_L and H_R for $\varepsilon_{CoFeB/IrMn}$ appears when $M_{IrMn}/M_{S(IrMn)} = 0$. The values of ε_K^{IrMn} stay low, and the barrier is observed between $\varphi = 90°$ and $180°$ under H_L, while it is between $\varphi = 0°$ and $90°$ under H_R. The existence of $\varepsilon_{CoFeB/IrMn}$ associated with different M_{IrMn} values is not sufficient for the existence of EB, and EB also requires a mechanism for fixing the direction of an exchange field produced on the FM through, for example, the pinning of domains within the AFM near the interface. The results show that M_{IrMn} is stabilized in the [100] direction by low enough ε_K^{IrMn}, regardless of φ, and the hard-axis directions can be detectable by ε_K^{IrMn} only when $\varepsilon_{CoFeB/IrMn}$ is high. According to the random-field model presented by Malozemoff [63,64] and a sophisticated model reported by Stiles and McMichael [65–67], the existence of domain walls in the AFM layers plays an important role in the EB effect, and H_E is proportional to the energy stored in the AFM domain walls. Thus, the AFM domain wall energy at the FM/AFM interface becomes proportional to φ for high enough K_{IrMn}/M_S.

When K_{eb} is oriented in the [110] direction and K_{IrMn}/M_S is constant, the maximum value of $M_{IrMn}/M_{S(IrMn)}$ decreases to ~ 0.7, and the $M_{IrMn}/M_{S(IrMn)}$ peak and zero values shift by $45°$ as compared with $K_{eb}||[100]$. Moreover, the calculated $\langle\varphi_{IrMn}\rangle$ value equals $\sim 45°$ when φ increases from $0°$ to $90°$ and then linearly increases for larger φ by $\langle\varphi_{IrMn}\rangle = \varphi + 45°$. The minimum value of $\varepsilon_{CoFeB/IrMn}$ under H_L is enhanced to ~ -0.8 and stabilized between $\varphi = 0°$ and $112.5°$, and under H_R, the maximum value of $\varepsilon_{CoFeB/IrMn}$ is lower, and
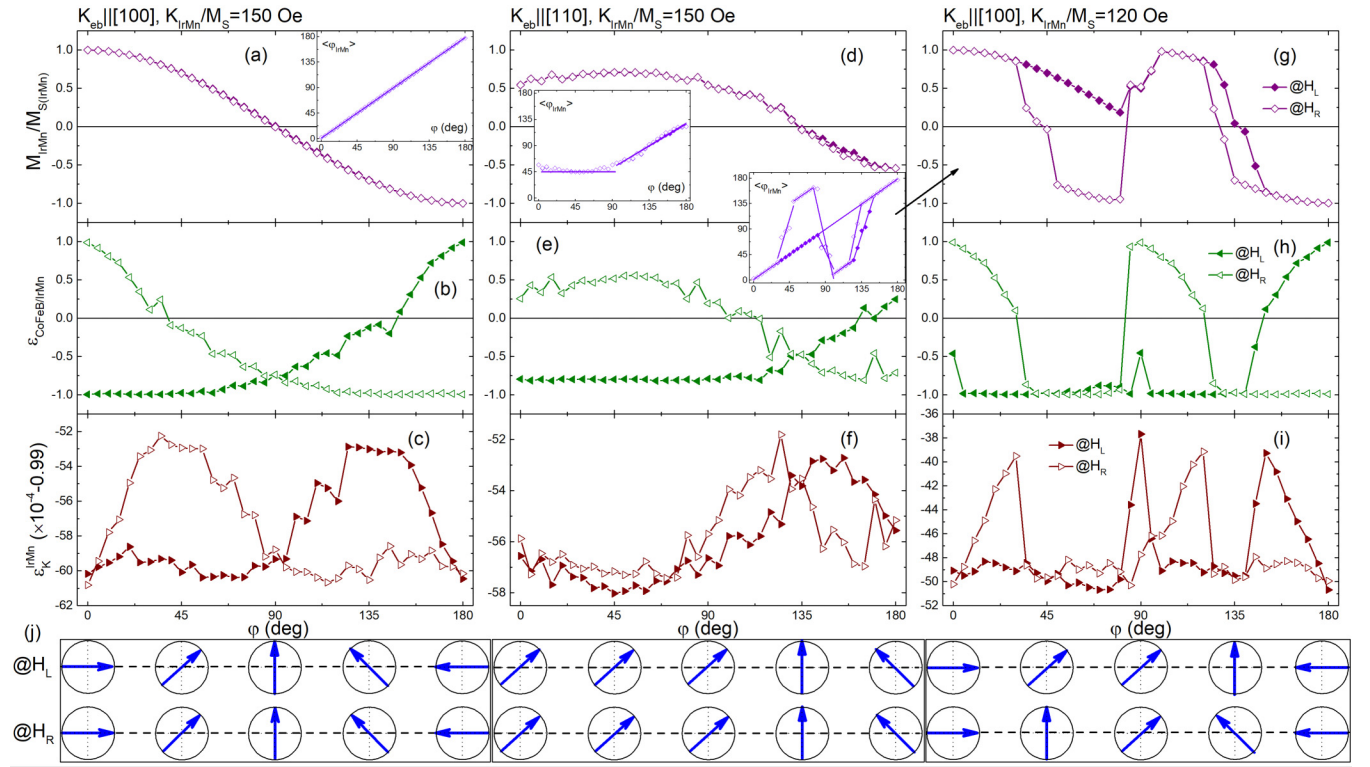
FIG. 6. (a), (d), and (g) Uncompensated antiferromagnet (AFM) magnetization ($M_{IrMn}/M_{S(IrMn)}$), (b), (e), and (h) CoFeB/IrMn interfacial exchange energy density ($\varepsilon_{CoFeB/IrMn}$), and (c), (f), and (i) AFM anisotropy energy density (ε_K^{IrMn}) under the coercive fields at the descending (H_L, solid) and ascending (H_R, open) branches as a function of φ for selected directions of unidirectional anisotropy (K_{eb}) and selected values of AFM anisotropic field (K_{IrMn}/M_S). (j) Effective AFM magnetization directions at $\varphi = 0°$, $45°$, $90°$, $135°$, and $180°$. The insets show the φ dependence of the average AFM magnetization direction ($\langle \varphi_{IrMn} \rangle$).

the degenerate state under H_L and H_R for $\varepsilon_{CoFeB/IrMn}$ still corresponds to $M_{IrMn}/M_{S(IrMn)} = 0$ (at $\varphi = 135°$). The ε_K^{IrMn} values also stay in the low-value range, and the energy barriers of ε_K^{IrMn} under H_L and H_R both occur between $\varphi = 90°$ and $180°$, resulting in a slight irreversibility of $M_{IrMn}/M_{S(IrMn)}$ observed around $\varphi = 157.5°$. When K_{IrMn}/M_S decreases from 150 to 120 Oe and K_{eb} is pointing in the [100] direction, the behaviors of $M_{IrMn}/M_{S(IrMn)}$, $\langle \varphi_{IrMn} \rangle$, $\varepsilon_{CoFeB/IrMn}$, and ε_K^{IrMn} are distinct from those for $K_{IrMn}/M_S = 150$ Oe. The value of $M_{IrMn}/M_{S(IrMn)}$ decreases from $+1$ with increasing φ from $0°$ to $80°$, and a large irreversibility between H_L and H_R is observed when φ is $>30°$. Then $M_{IrMn}/M_{S(IrMn)}$ increases with increasing φ from $80°$ to $100°$ and decreases with increasing φ from $100°$ to $120°$, with a reversibility between H_L and H_R. With increasing φ from $120°$ to $150°$, $M_{IrMn}/M_{S(IrMn)}$ sharply decreases from positive to negative, accompanied with an irreversibility between H_L and H_R. Finally, the irreversibility vanishes, and $M_{IrMn}/M_{S(IrMn)}$ smoothly decreases to -1 with further increasing φ to $180°$. The results of $\varepsilon_{CoFeB/IrMn}$ and ε_K^{IrMn} indicate that the AFM spins are frozen when the field is applied along one of the easy-axis directions of K_{IrMn}, such as $0°$, $90°$, and $180°$. Otherwise, the AFM spins become rotatable in the hard-axis direction, designating that the energy barriers in the enhanced ε_K^{IrMn} can effectively affect the AFM spin reversal and result in complex behaviors of H_E and H_C with respect to φ. Therefore, a possible origin of the fourfold and uniaxial anisotropy terms is the nonrigid spin structure of

the AFM layer. Rotation of the FM layer magnetization may cause canting of the AFM spins. It was theoretically shown that these rotations of the AFM spins away from an AFM easy axis may lead to high-order terms in the Fourier expansion of the exchange anisotropy [11,68].

V. CONCLUSIONS

In summary, an amorphous-CoFeB/epitaxial-IrMn bilayer was fabricated, and the IrMn anisotropy was characterized to be cubically symmetric. The angular (φ) dependence of H_E and H_C at room temperature after cooling under a field applied parallel to or by $45°$ with the [100] direction is studied. A unidirectional symmetry of H_E vs φ with the symmetric axis parallel to K_{eb} is observed, while the higher-order terms must be used to fit the experimental data. The Monte Carlo simulation was also performed to reproduce the experimental findings and elucidate the mechanisms. The large K_{IrMn} generates a low enough energy potential to trap the AFM spins frozen near the FC direction, and K_{IrMn} in other easy-axis directions cannot contribute to EB with φ, which is interpreted by the calculated results of uncompensated AFM magnetization at the FM/AFM interface and energies of interfacial exchange interaction and AFM anisotropy. This has been evidenced by decreasing the K_{IrMn} value by hand as the input parameter in the simulation, where the H_E and H_C behaviors with φ show responses to each easy- and hard-axis direction

of K_{IrMn}. On the other hand, K_{CoFeB} plays a crucial role in H_C, which also depends on φ. Our results shed light on some of the open questions in EB such as reversal asymmetry and especially the relationship between EB and AFM anisotropy. This understanding will provide profound insight into the EB phenomena in FM/AFM bilayers with a fully epitaxial AFM layer and certainly open prospects for future applications in magnetic devices.

[1] W. H. Meiklejohn and C. P. Bean, New magnetic anisotropy, Phys. Rev. **102**, 1413 (1956).

[2] J. Nogués, J. Sort, V. Langlais, V. Skumryev, S. Suriñach, J. S. Muñoz, and M. D. Baró, Exchange bias in nanostructures, Phys. Rep. **422**, 65 (2005).

[3] S. S. P. Parkin and V. S. Speriosu, in *Magnetic Properties of Low-Dimensional Systems II*, edited by L. M. Falicov, F. Mejia-Lira, and J. L. Morán-López (Springer-Verlag, Berlin, 1990), Vol. 50, p. 110.

[4] W. H. Meiklejohn and C. P. Bean, New magnetic anisotropy, Phys. Rev. **105**, 904 (1957).

[5] X. W. Wu, T. Ambrose, and C. L. Chien, Exchange bias and spin-valve structures using amorphous ferromagnetic $Co_{65}Mo_2B$ layers, Appl. Phys. Lett. **72**, 2176 (1998).

[6] J. W. Cai, K. Liu, and C. L. Chien, Exchange coupling in the paramagnetic state, Phys. Rev. B **60**, 72 (1999).

[7] T. Ambrose, R. L. Sommer, and C. L. Chien, Angular dependence of exchange coupling in ferromagnet/antiferromagnet bilayers, Phys. Rev. B **56**, 83 (1997).

[8] N. J. Gökemeijer, T. Ambrose, and C. L. Chien, Long-Range Exchange Bias Across a Spacer Layer, Phys. Rev. Lett. **79**, 4270 (1997).

[9] H. Xi, M. H. Kryder, and R. M. White, Study of the angular-dependent exchange coupling between a ferromagnetic and an antiferromagnetic layer, Appl. Phys. Lett. **74**, 2687 (1999).

[10] J. Geshev, L. G. Pereira, and J. E. Schmidt, Rotatable anisotropy and coercivity in exchange-bias bilayers, Phys. Rev. B **66**, 134432 (2002).

[11] I. N. Krivorotov, C. Leighton, J. Nogués, I. K. Schuller, and E. Dan Dahlberg, Relation between exchange anisotropy and magnetization reversal asymmetry in Fe/MnF_2 bilayers, Phys. Rev. B **65**, 100402(R) (2002).

[12] E. Jiménez, J. Camarero, J. Sort, J. Nogués, N. Mikuszeit, J. M. García-Martín, A. Hoffmann, B. Dieny, and R. Miranda, Emergence of noncollinear anisotropies from interfacial magnetic frustration in exchange-bias systems, Phys. Rev. B **80**, 014415 (2009).

[13] Y. J. Tang, B. F. P. Roos, T. Mewes, A. R. Frank, M. Rickart, M. Bauer, S. O. Demokritov, B. Hillebrands, X. Zhou, B. Q. Liang, X. Chen, and W. S. Zhan, Structure and magnetic properties of exchange-biased polycrystalline Fe/MnPd bilayers, Phys. Rev. B **62**, 8654 (2000).

[14] W. Zhang and K. M. Krishnan, Epitaxial exchange-bias systems: from fundamentals to future spin-orbitronics, Mater. Sci. Eng. R **105**, 1 (2016).

[15] Y. Ijiri, T. C. Schulthess, J. A. Borchers, P. J. van der Zaag, and R. W. Erwin, Link between Perpendicular Coupling and Exchange Biasing in Fe_3O_4/Coo Multilayers, Phys. Rev. Lett. **99**, 147201 (2007).

[16] M. Finazzi, M. Portalupi, A. Brambilla, L. Duò, G. Ghiringhelli, F. Parmigiani, M. Zacchigna, M. Zangrando, and F. Ciccacci, Magnetic anisotropy of NiO epitaxial thin films on Fe(001), Phys. Rev. B **69**, 014410 (2004).

[17] J. Nogués, T. J. Moran, D. Lederman, and I. K. Schuller, Role of interfacial structure on exchange-biased FeF_2-Fe, Phys. Rev. B **59**, 6984 (1999).

[18] Q. F. Zhan and K. M. Krishnan, In-plane reorientation of magnetization in epitaxial exchange biased Fe/MnPd bilayers, Appl. Phys. Lett. **96**, 112506 (2010).

[19] Q. F. Zhan, W. Zhang, and K. M. Krishnan, Antiferromagnetic layer thickness dependence of the magnetization reversal in the epitaxial MnPd/Fe exchange bias system, Phys. Rev. B **83**, 094404 (2011).

[20] P. Blomqvist, K. M. Krishnan, S. Srinath, and S. G. E. te Velthuis, Magnetization processes in exchange-biased MnPd/Fe bilayers studied by polarized neutron reflectivity, J. Appl. Phys. **96**, 6523 (2004).

[21] W. Zhang, M. E. Bowden, and K. M. Krishnan, Competing effects of magnetocrystalline anisotropy and exchange bias in epitaxial Fe/IrMn bilayers, Appl. Phys. Lett. **98**, 092503 (2011).

[22] S. G. Wang, A. Kohn, C. Wang, A. K. Petford-Long, S. Lee, R. Fan, J. P. Goff, L. J. Singh, Z. H. Barber, and R. C. C. Ward, Exchange bias in epitaxial $Fe/Ir_{0.2}Mn_{0.8}$ bilayers grown on MgO (001), J. Phys. D: Appl. Phys. **42**, 225001 (2009).

[23] H. H. Huang, C. Y. Yang, and C. H. Lai, Reorientation of exchange anisotropy in epitaxial (002) IrMn/CoFe system, J. Appl. Phys. **105**, 07D724 (2009).

[24] Y. Xie, Q. Zhan, Y. Hu, X. Hu, X. Chi, C. Zhang, H. Yang, W. Xie, X. Zhu, J. Gao, W. Cheng, D. Jiang, and R. W. Li, Magnetocrystalline anisotropy imprinting of an antiferromagnet on an amorphous ferromagnet in FeRh/CoFeB heterostructures, NPG Asia Mater. **12**, 67 (2020).

[25] C. Zhang, Y. Xie, Q. Zhan, and Y. Hu, Anisotropic coercivity and the effects of interlayer exchange coupling in CoFeB/FeRh bilayers, Phys. Rev. B **103**, 014445 (2021).

[26] T. Hajiri, T. Yoshida, S. Jaiswal, M. Filianina, B. Borie, H. Ando, H. Asano, H. Zabel, and M. Kläui, Magnetization switching behavior with competing anisotropies in epitaxial Co_3FeN/MnN exchange-coupled bilayers, Phys. Rev. B **94**, 184412 (2016).

[27] S. S. P. Parkin, C. Kaiser, A. Panchula, P. M. Rice, B. Hughes, M. Samant, and S. H. Yang, Giant tunneling magnetoresistance

at room temperature with MgO (100) tunnel barriers, Nature Mater. **3**, 862 (2004).

[28] S. Ikeda, K. Miura, H. Yamamoto, K. Mizunuma, H. D. Gan, M. Endo, S. Kanai, J. Hayakawa, F. Matsukura, and H. Ohno, A perpendicular-anisotropy CoFeB-MgO magnetic tunnel junction, Nature Mater. **9**, 721 (2010).

[29] A. Fernández-Pacheco, E. Vedmedenko, F. Ummelen, R. Mansell, D. Petit, and R. P. Cowburn, Symmetry-breaking interlayer Dzyaloshinskii-Moriya interactions in synthetic antiferromagnets, Nat. Mater. **18**, 679 (2019).

[30] S. Peng, D. Zhu, W. Li, H. Wu, A. J. Grutter, D. A. Gilbert, J. Lu, D. Xiong, W. Cai, P. Shafer, K. L. Wang, and W. Zhao, Exchange bias switching in an antiferromagnet/ferromagnet bilayer driven by spin-orbit torque, Nat. Electron. **3**, 757 (2020).

[31] Y. W. Oh, S. H. Chris Baek, Y. M. Kim, H. Y. Lee, K. D. Lee, C. G. Yang, E. S. Park, K. S. Lee, K. W. Kim, G. Go, J. R. Jeong, B. C. Min, H. W. Lee, K. J. Lee, and B. G. Park, Field-free switching of perpendicular magnetization through spin-orbit torque in antiferromagnet/ferromagnet/oxide structures, Nature Nanotech. **11**, 878 (2016).

[32] B. Liu, B. Wang, T. Nie, Y. Xie, H. Yang, G. Li, J. Pan, and R. W. Li, Effect of isothermal crystallization in antiferromagnetic IrMn on the formation of spontaneous exchange bias, Appl. Phys. Lett. **118**, 252404 (2021).

[33] D. Xiong, S. Peng, J. Lu, W. Li, H. Wu, Z. Li, H. Cheng, Y. Wang, C. H. Back, K. L. Wang, and W. Zhao, Modulation of thermal stability and spin-orbit torque in IrMn/CoFeB/MgO structures through atom thick W insertion, Appl. Phys. Lett. **117**, 212401 (2020).

[34] E. Albisetti, G. Scaramuzzi, C. Rinaldi, M. Cantoni, R. Bertacco, and D. Petti, Temperature dependence of the magnetic properties of IrMn/CoFeB/Ru/CoFeB exchange biased synthetic antiferromagnets, Materials **13**, 387 (2020).

[35] M. Raju, S. Chaudhary, and D. K. Pandya, Magnetic annealing of the ion-beam sputtered IrMn/CoFeB bilayers-positive exchange bias and coercivity behavior, Eur. Phys. J. B **86**, 491 (2013).

[36] N. Mohanta, E. Dagotto, and S. Okamoto, Topological Hall effect and emergent skyrmion crystal at manganite-iridate oxide interfaces, Phys. Rev. B **100**, 064429 (2019).

[37] J. d'Albuquerque e Castro, D. Altbir, J. C. Retamal, and P. Vargas, Scaling Approach to the Magnetic Phase Diagram of Nanosized Systems, Phys. Rev. Lett. **88**, 237202 (2002).

[38] Y. Hu and A. Du, The effect of field-cooling strength and interfacial coupling on exchange bias in a granular system of ferromagnetic nanoparticles embedded in an antiferromagnetic matrix, J. Appl. Phys. **102**, 113911 (2007).

[39] S. Yang and Y. Hu, Inverse dependence of exchange bias and coercivity on cooling field caused by interfacial randomization in nanosystems with Co sparsely distributed in $CoFe_2O_4$ matrix, J. Mater. Sci. Technol. **98**, 258 (2022).

[40] Z. C. Huang, Y. Zhai, Y. X. Lu, G. D. Li, P. K. J. Wong, Y. B. Xu, Y. X. Xu, and H. R. Zhai, The interface effect of the magnetic anisotropy in ultrathin epitaxial Fe_3O_4 film, Appl. Phys. Lett. **92**, 113105 (2008).

[41] T. J. Moran, J. Nogués, D. Lederman, and I. K. Schuller, Perpendicular coupling at Fe-FeF_2 interfaces, Appl. Phys. Lett. **72**, 617 (1998).

[42] J. Wu, J. Choi, A. Scholl, A. Doran, E. Arenholz, Y. Z. Wu, C. Won, C. Hwang, and Z. Q. Qiu, Element-specific study of

the anomalous magnetic interlayer coupling across NiO spacer layer in Co/NiO/Fe/Ag(001) using XMCD and XMLD, Phys. Rev. B **80**, 012409 (2009).

[43] J. Wu, J. S. Park, W. Kim, E. Arenholz, M. Liberati, A. Scholl, Y. Z. Wu, C. Hwang, and Z. Q. Qiu, Direct Measurement of Rotatable and Frozen CoO Spins in Exchange Bias System of CoO/Fe/Ag(001), Phys. Rev. Lett. **104**, 217204 (2010).

[44] W. Zhang and K. M. Krishnan, Spin-flop coupling and rearrangement of bulk antiferromagnetic spins in epitaxial exchange-biased Fe/MnPd/Fe/IrMn multilayers, Phys. Rev. B **86**, 054415 (2012).

[45] P. J. Jensen and H. Dreyssé, In-plane magnetic reorientation in coupled ferro- and antiferromagnetic thin films, Phys. Rev. B **66**, 220407(R) (2002).

[46] A. K. Nayak, M. Nicklas, S. Chadov, P. Khuntia, C. Shekhar, A. Kalache, M. Baenitz, Y. Skourski, V. K. Guduru, A. Puri, U. Zeitler, J. M. D. Coey, and C. Felser, Design of compensated ferrimagnetic Heusler alloys for giant tunable exchange bias, Nature Mater. **14**, 679 (2015).

[47] J. Nogues, D. Legerman, T. J. Moran, and I. K. Schuller, Positive Exchange Bias in FeF_2-Fe Bilayers, Phys. Rev. Lett. **76**, 4624 (1996).

[48] D. Y. Kim, C. G. Kim, C. O. Kim, M. Shibata, M. Tsunoda, and M. Takahashi, Angular dependence of exchange bias and coercive field in CoFe/MnIr epitaxial bilayers, IEEE Trans. Magn. **41**, 2712 (2005).

[49] T. Mewes, H. Nembach, M. Rickart, S. O. Demokritov, J. Fassbender, and B. Hillebrands, Angular dependence and phase diagrams of exchange-coupled epitaxial $Ni_{81}Fe_{19}/Fe_{50}Mn_{50}$(001) bilayers, Phys. Rev. B **65**, 224423 (2002).

[50] S. Dubourg, J. F. Bobo, B. Warot, E. Snoeck, and J. C. Ousset, Complex angular dependence of exchange bias on (001) epitaxial NiO-Co bilayers, Eur. Phys. J. B **45**, 175 (2005).

[51] T. Hajiri, T. Yoshida, M. Filianina, S. Jaiswal, B. Borie, H. Asano, H. Zabel, and M. Kläui, 45° sign switching of effective exchange bias due to competing anisotropies in fully epitaxial Co_3FeN/MnN bilayers, J. Phys.: Condens. Matter **30**, 015806 (2017).

[52] R. H. Kodama, S. A. Makhlouf, and A. E. Berkowitz, Finite Size Effects in Antiferromagnetic Nio Nanoparticles, Phys. Rev. Lett. **79**, 1393 (1997).

[53] F. Radu, A. Westphalen, K. Theis-Bröhl, and H. Zabel, Quantitative description of the azimuthal dependence of the exchange bias effect, J. Phys.: Condens. Matter **18**, L29 (2006).

[54] J. Camarero, J. Sort, A. Hoffmann, J. M. García-Martín, B. Dieny, R. Miranda, and J. Nogués, Origin of the Asymmetric Magnetization Reversal Behavior in Exchange-Biased Systems: Competing Anisotropies, Phys. Rev. Lett. **95**, 057204 (2005).

[55] M. R. Fitzsimmons, P. Yashar, C. Leighton, I. K. Schuller, J. Nogués, C. F. Majkrzak, and J. A. Dura, Asymmetric Magnetization Reversal in Exchange-Biased Hysteresis Loops, Phys. Rev. Lett. **84**, 3986 (2000).

[56] Y. Hu, F. Shi, G. Z. Wu, N. Jia, Y. Liu, and A. Du, Origin of the angular dependent magnetization reversal processes in exchange-biased bilayers, J. Phys. Soc. Jpn. **82**, 064602 (2013).

[57] E. Jiménez, J. Camarero, J. Sort, J. Nogués, A. Hoffmann, F. J. Teran, P. Perna, J. M. García-Martín, B. Dieny, and R. Miranda, Highly asymmetric magnetic behavior in exchange biased

systems induced by noncollinear field cooling, Appl. Phys. Lett. **95**, 122508 (2009).

[58] S. Roy, M. R. Fitzsimmons, S. Park, M. Dorn, O. Petracic, I. V. Roshchin, Z. P. Li, X. Batlle, R. Morales, A. Misra, X. Zhang, K. Chesnel, J. B. Kortright, S. K. Sinha, and I. K. Schuller, Depth Profile of Uncompensated Spins in an Exchange Bias System, Phys. Rev. Lett. **95**, 047201 (2005).

[59] H. Ohldag, A. Scholl, F. Nolting, E. Arenholz, S. Maat, A. T. Young, M. Carey, and J. Stöhr, Correlation between Exchange Bias and Pinned Interfacial Spins, Phys. Rev. Lett. **91**, 017203 (2003).

[60] F. Radu, M. Etzkorn, T. Schmitte, R. Siebrecht, A. Schreyer, K. Westerholt, and H. Zabel, Asymmetric magnetization reversal on exchange biased CoO/Co bilayers, J. Magn. Magn. Mater. **240**, 251 (2002).

[61] F. Radu, M. Etzkorn, R. Siebrecht, T. Schmitte, K. Westerholt, and H. Zabel, Interfacial domain formation during magnetization reversal in exchange-biased CoO/Co bilayers, Phys. Rev. B **67**, 134409 (2003).

[62] J. McCord, R. Schäfer, R. Mattheis, and K. U. Barholz, Kerr observations of asymmetric magnetization reversal processes in CoFe/IrMn bilayer systems, J. Appl. Phys. **93**, 5491 (2003).

[63] A. P. Malozemoff, Random-field model of exchange anisotropy at rough ferromagnetic-antiferromagnetic interfaces, Phys. Rev. B **35**, 3679 (1987).

[64] A. P. Malozemoff, Mechanisms of exchange anisotropy, J. Appl. Phys. **63**, 3874 (1988).

[65] M. D. Stiles and R. D. McMichael, Model for exchange bias in polycrystalline ferromagnet-antiferromagnet bilayers, Phys. Rev. B **59**, 3722 (1999).

[66] M. D. Stiles and R. D. McMichael, Temperature dependence of exchange bias in polycrystalline ferromagnet-antiferromagnet bilayers, Phys. Rev. B **60**, 12950 (1999).

[67] M. D. Stiles and R. D. McMichael, Coercivity in exchange-bias bilayers, Phys. Rev. B **63**, 064405 (2001).

[68] J. V. Kim, R. L. Stamps, B. V. McGrath, and R. E. Camley, Angular dependence and interfacial roughness in exchange-biased ferromagnetic/antiferromagnetic bilayers, Phys. Rev. B **61**, 8888 (2000).